CHAPTER 5

EQUIVALENT CIRCUIT APPROACH FOR RF ANALYSIS OF MILO

5.1 Introduction

Metal disc-loaded coaxial cylindrical waveguiding structures are frequently used for microwave devices as the slow-wave and fast-wave RF propagating structures at the microwave and millimeter wave frequency ranges. In MILO, disc-loaded waveguide is used as its RF interaction structure with an additional coaxial metallic cylinder at its center. A disc-loaded coaxial waveguides structure is a periodic electromagnetic (EM) structure also finds applications in the passive devices, such as, filter, antenna, and antenna feed, mode converter, etc. as well as in the active devices as its RF interaction structures. Crossed-field high power microwave device — magnetically insulated line oscillator (MILO) which is a gigawatts level of RF oscillator also uses disc-loaded coaxial waveguiding structure as its RF interaction structure. Now-a-days, high power microwave devices employing intense relativistic electron beam are needed in many applications where direct energy weaponry is most important. MILO is being preferred leaving in all other high power microwave device because it reveals most important property for focusing electron beam. MILO doesn't require external magnetic field, due to which it seems to be compact and produces RF output power up to gigawatt range at lower microwave frequency range. This chapter is focussed on deriving dispersion relation and temporal growth rate for the coaxial disc loaded structure using equivalent circuit approach, that can be used as the RF interaction structure. This is revealed on extending the work outlined in previous chapter for beam present case.

5.2 Electromagnetic Analysis in the presence of Electron Beam

MILO device consists of coaxial cylindrical disc loaded periodic structure, in which metal disc is added radially inward with anode structure to form SWS cavity.

In this chapter, electromagnetic analysis for the MILO device considering equivalent circuit approach in the presence of electron beam is carried out, by modifying the analysis of previous chapter. It is worth noting that the effect of the presence of beam for a disc-loaded coaxial waveguide was included in the analyses due to [Dwivedi and Jain (2013)]. They used the modal field matching technique in the TM_{01} mode. This analysis is carried out to obtain the temporal growth rate, released RF energy, oscillation frequency and RF output power. For further rigorous and simplicity, here equivalent circuit approach is preferred.

5.2.1 Analytical Model

In the present chapter, the analysis of disc-loaded coaxial waveguide is extended, by taking into account the presence of beam due to explosive emission from the cathode surface. The application of a strong electric field results in plasma formation on the cathode surface due to surface flashover mechanism. The enhanced electric field then extracts a space-charge limited electron flow from this plasma [Miller (1998)]. MILO operates on the principle of load limited magnetically insulated flow. During magnetic insulation, electron drift parallel to the cathode and an electron sheath is formed between the discs tip and cathode surface. This electron sheath equilibrium is known as the relativistic Brillouin flow (RBF). Electron sheath has both radial and axial electric field components in addition to the azimuthal magnetic field component. Present work is extended considering perturbation effect due to axial periodicity of discs, to estimate the mechanism of energy exchange between electron beam and RF, taking into account plasma frequency. During analysis consider a region of plasma (electron sheath) in equilibrium, but when this region is perturbed, space charge waves are formed, due to periodicity of disc and

lead to space charge instability. The axial periodic metal boundary of the anode structure will affect the outer radius of the electron sheath due to presence of radial field components. Axial field component perturbs space charge equilibrium. Here, considering that coaxial discs oscillate at *TM* waves, and three nonzero field components are radial electric field E_r, axial electric field E_z, and azimuthal magnetic field B_θ. Correlation between particles and different field components can be described using linearized Vlasov-Maxwell equation as:

$$\left.\begin{aligned} &\frac{\partial E_{r1}}{\partial z}-\frac{\partial E_{z1}}{\partial r}=-\frac{1}{c}\frac{\partial B_{\theta 1}}{\partial t} \\ &-\frac{\partial B_{\theta 1}}{\partial z}=\frac{1}{c}\frac{\partial E_{r1}}{\partial t} \\ &-\frac{1}{r}\frac{\partial}{\partial z}rB_{\theta 1}=\frac{4\pi}{c}J_{z1}+\frac{1}{c}\frac{\partial E_{z1}}{\partial t} \end{aligned}\right\} \tag{5.1}$$

Where, J_{z1} represents the perturbed (RF) axial current density,

$$J_{z1}\{x,t\}=-e\int v_b f_1\{x,p,t\}dp \ .$$

In above equation, $f_1\{x,p,t\}$ represents RF distribution function and can be expressed using floquet's theorem and Vlasov equation as [Lemke *et al.* (1997)],

$$f_1\{x,p,t\}=ie\frac{\partial f_0}{\partial p_z}\sum_{n=-\infty}^{\infty}\frac{E_{z,n}}{\Omega_n}\exp\left[i\left(\beta_n z-\omega t\right)\right].$$

Where, $\Omega_n=\omega-v_b\beta_n$ represents velocity shifted frequency. Different relevant EM field intensities components can be expressed by substituting Maxwell-Vlasov equations into Vlasov equation in conjunction with Floquet theorem [Lemke (1989)]:

The different components of *EM* field intensities, $E_{r,n}$, $E_{z,n}$, and $H_{\square,n}$, can be expressed as [Lemke(1989)]:

$$\left(\frac{1}{r}\frac{d}{dr}r\frac{d}{dr}+\Gamma_n^{*2}\right)E_{z,n}=0\ , \tag{5.2}$$

$$E_{r,n}=j\frac{\beta_n}{\gamma_n^2}\frac{dE_{z,n}}{dr}, \tag{5.3}$$

$$H_{\theta,n}=j\frac{k}{\gamma_n^2}\frac{dE_{z,n}}{dr} \tag{5.4}$$

Where, $\Gamma_n^{*2}=\gamma_n{}^2/[1-(\omega_p{}^2/\gamma_0{}^3\Omega_n{}^2)]$ is a constant in terms of the beam parameter and $\gamma_n{}^2=\frac{\omega^2}{c^2}-\beta_n{}^2$ is the radial propagation constant; $\beta_n=\beta_0+nh_0$ is the axial propagation constant and ω_p $(=(4\pi e\rho/m)^{1/2})$ is electron plasma frequency. Differential form of field expression (5.2) can be solved considering some relevant assumptions that the transverse electron motion in the perturbed state is negligible compared to corresponding axial motion. Thus expression for axial electric field in the presence of beam can be evaluated by solving second order differential equation using formulation of singular point transformation and Taylor series [Dwivedi and Jain (2013)],

1. $$E_{z,n}=A_nJ_n\{G_{2,n}r\}+B_nY_n\{G_{2,n}\,\mathrm{r}\}, \tag{5.5}$$

where, $G_{2,n}=(\Gamma_n^*r/\xi)^2-1/3.$

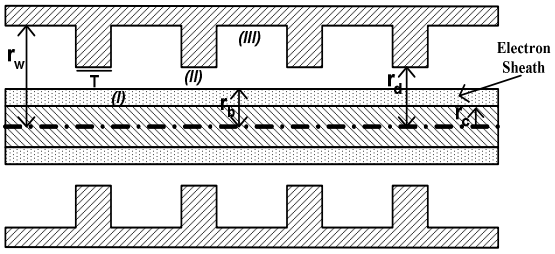

Figure 5.1: Schematic diagram of a disc-loaded coaxial waveguide structure with electron beam.

But the expression for axial electric field in the absence of beam can be written as:

$$E_z^I = \sum_{n=-\infty}^{\infty} [A_n^I J_0\{\gamma_n^I r\} + B_n^I Y_0\{\gamma_n^I r\}] \exp j(\omega t - \beta_n^I z) \ .$$

The electron beam present analysis of the coaxial disc loaded structure shown in Figure 5.1, is carried out through dividing the structure in three regions. Region I ($r_c \le r \le r_b$, $0 \le z \le \infty$) is cylindrical electron beam region around the coaxial cylindrical cathode of thickness r_b-r_c. Region II ($r_b \le r \le r_d$, $0 \le z \le \infty$) is the region between outer edge of the electron beam and tip of the metal discs. Region III ($r_d \le r \le r_w, 0 \le z \le (L-T)$) is the disc-occupied region between two consecutive metal disc as free space. Here, r_c is the radius of the central coaxial conductor, r_w is the waveguide-wall radius, r_d is the disc-hole radius with disc thickness T of the axial periodicity L and r_b is the outer beam radius. During analysis, it is assumed that the space harmonics of the travelling-wave being generated due to the axial periodicity of the structure and the modal harmonics of the standing wave caused due to the reflections of electromagnetic waves from the metal discs. Therefore, travelling waves will be present in the structure disc-free region (region I), between the central conductor and the metal discs, and the standing waves in the disc-occupied region (region II) of each unit cell, considered between two consecutive discs of the cylindrical coaxial waveguiding structure.

5.2.2 EM Boundary condition

The EM boundary conditions are described here to predict the structure characteristics, concern with either the axial or azimuthally components of the electric and magnetic field intensities at the interface between the two regions. The relevant boundary conditions referring to the continuity of the axial electric field intensity and

azimuthal component of magnetic field intensity at interface between region II and region III [Dwivedi and Jain (2012)]]:

$$\left.\begin{aligned} E_z^{II} &= E_z^{III} \\ H_\theta^{II} &= H_\theta^{III} \end{aligned}\right\} \text{ at } r = r_d;\ \ 0 < z < (L-T)\ . \tag{5.6}$$

The discontinuity of the tangential (azimuthal) component of magnetic field intensities at the interface, being equal to the surface current density:

$$H_\theta^{III} - H_\theta^{II} = J_z \ \text{ at } r = r_d;. \tag{5.7}$$

The normal components of electric field intensity are discontinuous at the interface and the amount of discontinuity being equal to surface charge density ρ_s given as:

$$E_r^{III} - E_r^{II} = \frac{\rho_s}{\varepsilon} \ \text{ at } r = r_b;\ \ 0 \le z < (L-T), \tag{5.8}$$

Assuming at the interface, $\varepsilon_r^{III} = \varepsilon_r^{II} = \varepsilon$

5.2.3 Electromagnetic field expression for region I

The region between coaxial cylindrical cathode and the outer radius of electron beam considered as region I. Traveling RF waves with all space harmonics are considered to be present in this region and contains no energy source because the electron motion is radially constant. Expression for axial component of electric field intensity may be written by invoking the boundary condition that, at metallic interface of discontinuity ($r = r_c$), then field expressions for beam present region I can be written as [Dwivedi and Jain (2012)]:

$$E_z^I = \sum_{n=-\infty}^{n=\infty} J_0\{G_{2n} r\} A_n^I e^{j\beta_n z} \ , \tag{5.9}$$

$$E_r^I = -j\sum_{n=-\infty}^{n=\infty}\frac{\beta_n G_{2,n}}{\gamma_n^2}J_1\{G_{2,n}\}\mathrm{A}_n^I e^{j\beta_n z}, \tag{5.10}$$

$$H_\theta^I = -j\omega\varepsilon\sum_{n=-\infty}^{n=\infty}\frac{G_{2,n}}{\gamma_n^2}J_1\{G_{2,n}\,\mathrm{r}\}A_n^I e^{j\beta_n z}, \tag{5.11}$$

5.2.4 Electromagnetic field expression for region II

Region II is the space between outer edge of the electron beam and tip of the metal discs in which, the travelling-waves will be present with all space harmonics due to the axial periodicity of the structure. Periodicity of discs perturbed the electron sheath equilibrium, results in the formation of space charge waves. This space charge wave oscillates at plasma frequency, which induces oscillations inside the cavity. Oscillations are induced due to acceleration and deceleration of electrons along the insulated sheath. Presence of radial electric field results in the formation of spokes. The field expression for region II can be written as [Dwivedi and Jain (2012)]:

$$\left.\begin{aligned} E_z^{II} &= \sum_{n=-\infty}^{\infty}[A_n^{II}J_0\{\gamma_n r\}+B_n^{II}Y_0\{\gamma_n r\}]\exp(j\beta_n z)\\ E_r^{II} &= \sum_{n=-\infty}^{\infty}\frac{j\beta_n}{\gamma_n^2}[A_n^{II}J_1\{\gamma_n^I r\}+B_n^{II}Y_1\{\gamma_n r\}]\exp(j\beta_n z)\\ H_\theta^{II} &= -j\omega\varepsilon\sum_{n=-\infty}^{\infty}\frac{1}{\gamma_n}[A_n^{II}J_1\{\gamma_n r\}+B_n^{II}Y_1\{\gamma_n r\}]\exp(j\beta_n z)\end{aligned}\right\} \tag{5.12}$$

Considering boundary condition at the interface where presence of space charge wave at the surface of insulated sheath between region I and II, modify the expression for axial and radial electric field. Invoking boundary condition, $E_z^I(r_b)=E_z^{II}(r_b)$, field constants A_n^{II} and B_n^{II} can be calculated as [Minami *et al.*(1990), Amin *et al.*(1995)]:

$$\left.\begin{aligned} A_n^{II} &= (1-bJ_0\{\gamma_n r_b\}Y_0\{\gamma_n r_b\})A_n^I\\ B_n^{II} &= bJ_0^2\{\gamma_n r_b\}A_n^I; b=c^2(k^2-\beta_n^2/(\omega-\gamma_n v_b))^2 I_b\end{aligned}\right\} \tag{5.13}$$

In above equation, I_b is beam current. Recasting equation (5.12) by substituting equation (5.13), the field equation for region II can be written in terms of field constant of region I.

$$\left.\begin{aligned} E_z^{II} &= -\sum_{n=-\infty}^{n=\infty} \varphi_n[((1-bJ_0\{\gamma_n r_b\}Y_0\{\gamma_n r_b\})J_0\{\gamma_n r\}+bJ_0^2\{\gamma_n r_b\}Y_0\{\gamma_n r\})]A_n^I e^{j\beta_n z} \\ E_r^{II} &= j\sum_{n=-\infty}^{n=\infty}\left[\frac{\varphi_n\beta_n}{\gamma_n^2}((1-bJ_0\{\gamma_n r_b\}Y_0\{\gamma_n r_b\})J_1\{\gamma_n r\}+bJ_0^2\{\gamma_n r_b\}Y_1\{\gamma_n r\})\right]A_n^I e^{j\beta_n z} \\ H_\theta^{II} &= -j\omega\varepsilon\sum_{n=-\infty}^{n=\infty}\frac{\phi_n}{\gamma_n}[(1-bJ_0\{\gamma_n r_b\}Y_0\{\gamma_n r_b\})J_1\{\gamma_n r\}+bJ_0^2\{\gamma_n r_b\}Y_1\{\gamma_n r\}]A_n^I e^{j\beta_n z} \end{aligned}\right\} \quad (5.14)$$

where, I_b is beam current, $\varphi_n = Y_0\{G_{2,n}r\}/J_0\{G_{2,n}r\}$ and $b = c^2(k^2-\beta_n^2/(\omega-\gamma_n v_b))^2 I_b$.

5.2.5 Electromagnetic field expression for region III

Region III is the free space region between two consecutive discs separated by an axial distance (*L-T*). In this region stationary waves are supported due to the reflections from the metal discs, accommodating an integral number of half guide wavelength as, $(L-T) = m\lambda_m^{III}/2$, where *m* represents the model space harmonics (*m* = 1, 2, 3, ...). The travelling waves will not be present in this region. The axial electric field intensity and azimuthal magnetic field in region III for the stationary wave supported between discs, is given as [Dwivedi and Jain (2012)]:

$$E_z^{III} = \sum_{m=1}^{\infty} E_{z,m}^{III} = \sum_{m=1}^{\infty} X_0\{\gamma_m^{III} r\}A_m^{III}\exp(j\omega t)\sin\beta_m^{III} z, \quad (5.15)$$

where, $X_0\{\gamma_m^{III} r\} = Y_0\{\gamma_m^{III} r_w\}J_0\{\gamma_m^{III} r\} - J_0\{\gamma_m^{III} r_w\}Y_0\{\gamma_m^{III} r\}$,

$$E_r^{III} = \sum_{m=1}^{\infty}\frac{j\beta_m^{III}}{\gamma_m^{III}}A_m^{III}X_0'\{\gamma_m^{III} r\}\exp(j\omega t)\sin(\beta_m^{III} z), \quad (5.16)$$

$$H_\theta^{III} = \sum_{m=1}^{\infty} H_{\theta,m}^{III} = \sum_{m=1}^{\infty} A_m^{III}X_0'\{\gamma_m^{III} r\}\exp(j\omega t)\sin(\beta_m^{III} z), \quad (5.17)$$

where, $X_0'\{\gamma_m^{III} r\} = Y_0\{\gamma_m^{III} r_w\} J_1\{\gamma_m^{III} r\} - J_0\{\gamma_m^{III} r_w\} Y_1\{\gamma_m^{III} r\}$.

5.3. Equivalent Circuit Approach

Equivalent circuit is an alternative analytical approach for analyzing an EM structure. In this approach, the actual EM structure is treated as a transmission line characterized by a set of four distributed line parameters. Using equivalent circuit analysis slow wave structure is replaced by a lumped parameter transmission line whose inductance and capacitance per unit length has been calculated which are used to calculate the phase velocity and characteristics impedance of the structure.

5.3.1 Equivalent shunt capacitance per unit length

In this section, authors have analyzed the coaxial disc loaded structure, in the slow-wave operating regime suitable as RF interaction structure for slow-wave high power microwave device (MILO). Using equivalent circuit approach explained in previous chapter, telegraphic equation has been derived taken into account circuit current and voltage along the interaction length in the *TM* operating mode. During equivalent circuit analysis slow wave structure is replaced by a lumped parameter transmission line whose inductance and capacitance per unit length has been calculated which are used to calculate the phase velocity and characteristics impedance of the structure. Further, using this approach, the dispersion relation and temporal growth rate is used to investigate the oscillation process inside the RF structure in terms of structure parameters. Expression for the equivalent shunt capacitance per unit length for the structure can be obtained using the 'current' telegraphist's equation. Here, same expression is used as mentioned in previous chapter.

$$C_e = \frac{\beta_n}{\omega}\frac{I_z}{V}. \tag{5.18}$$

Here, authors follow the same steps for finding the ratio of axial current to voltage as explained in previous chapter. In this chapter, authors consider beam present field expressions for different regions. Considering boundary condition between interface of two regions, express the axial electric field in terms of axial current and voltage. Then equating, both the expression, find the ratio of axial current to voltage. For this purpose, the field expressions (5.14) and (5.15) are inserted into the first boundary condition explained in Equation (5.6). After rearranging, multiplied both sides by $\sin(\beta_m^{III} z)$ and integrating further within the limit $0 \le z < (L-T)$ as well as using orthogonal property of trigonometric function results in:

$$A_m^{III} = \sum_{n=-\infty}^{\infty} X_{nm}^{*}\{\gamma_n r\} A_n^{I} \quad ,$$

where, $$X_{nm}^{*}\{\gamma_n r\} = B_1\{\gamma_n r\} \times S \times (2/(L-T))/(X_0\{\gamma_m^{III} r\}\exp(j\omega t)) \quad , \tag{5.19}$$

$$B_1\{\gamma_n r\} = -\sum_{n=-\infty}^{\infty} \phi_n \left[[(1 - bJ_0\{\gamma_n r_b\} Y_0\{\gamma_n r_b\}) J_0\{\gamma_n r\} + bJ_0^2\{\gamma_n r_b\} Y_0\{\gamma_n r\}] \right], \tag{5.20}$$

$$S = \left\{ \frac{\beta_m^{III}(1-(-1)^m \exp j\beta_n^I (L-T))}{\left(\beta_m^{III}\right)^2 - (\beta_n^I)^2} \right\}.$$

Due to the cavities coupled by means of capacitors a relation between field constant in region III and in region I is derived. To evaluate the capacitance field constant exists between the tip of discs and cathode, in terms of axial current, we used boundary condition (5.7). Thus substituting expression (5.14) and (5.17) into define boundary condition. Resulting expression is solved using Equation (5.19) by replacing field constant A_m^{III}. Then, multiplying both sides by $\sin(\beta_m^{III} z)$ and integrating within limit $0 \le z < (L-T)$ using orthogonal property of the trigonometric function. Finally, recasting, expression can be written as:

$$A_n^I = R_{nm}^*\{\gamma_n r\} I_z\,, \tag{5.21}$$

$$R_{nm}^*\{\gamma_n r\} = \sum_{n=-\infty}^{\infty} \frac{X_0\{\gamma_m^{III} r\}\gamma_m^{III}(L-T)^2\cos(\beta_m^{III}(L-T))}{2\pi r_d S(j\omega\varepsilon)\left[B_1\{\gamma_n r\}X_0'\{\gamma_m^{III} r\} + X_0\{\gamma_m^{III} r\}\gamma_m^{III}(L-T)^2 B_2\{\gamma_n r\}\right]},$$

In above expression,

$$B_2\{\gamma_n r\} = \phi_n / \gamma_n\left[(1-bJ_0\{\gamma_n r_b\}Y_0\{\gamma_n r_b\})J_1\{\gamma_n r\} + bJ_0^2\{\gamma_n r_b\}Y_1\{\gamma_n r\}\right].$$

Finally, relation between axial electric field intensity in terms of axial current is being derived, considering Equation (5.21). Substituting this equation in (5.9), expression for axial electric field intensity can be written as,

$$E_z^I = \sum_{n=-\infty}^{\infty} R_{nm}^* J_0\{G_{2n} r_c\}\exp(j\beta_n z) I_z = P_{nm}^*\{\gamma_n r\} I_z\,, \tag{5.22}$$

where,
$$P_{nm}^*\{\gamma_n r\} = \sum_{n=-\infty}^{\infty} R_{nm}^*\{\gamma_n r\} J_0\{G_{2n} r_c\}\,. \tag{5.23}$$

Now, the axial electric field intensity can be written in terms of circuit potential as:

$$E_z^I = j\left(\frac{\gamma_n'^2}{\beta_n'}\right)V\,. \tag{5.24}$$

Equating (5.22) and (5.24), to find ratio of axial current to voltage and further substituted in (5.18) to obtain an expression for the shunt capacitance per unit length in terms of structure parameters as:

$$C_e\{\gamma_n r\} = \frac{j}{\omega}\left[\frac{(\gamma_n')^2}{P_{nm}^*\{\gamma_n r\}}\right]. \tag{5.25}$$

5.3.2 Equivalent Series Inductance per unit length

Series inductance per unit length of the equivalent transmission line for the structure under consideration can be obtained using the 'voltage' telegraphist's equation explained in previous chapter.

$$L_e = \left(\frac{\beta_n}{\omega}\right)\frac{V}{I_\theta}\,. \tag{5.26}$$

To find the ratio of circuit potential and circuit current, V/I_θ, the relation between the field constants, A_m^{III} and A_n^I is required. Inside inductance energy is stored in the form of magnetic field. Field expressions from Equations (5.14) and (5.17) are substituted in the second boundary condition of Equation (5.6). After substituting, multiply both sides by $\sin(\beta_m^{III} z)$ and integrating within limit $0 \le z < (L-T)$ using orthogonal property of the trigonometric function, to obtain relation between various field constants A_m^{III} in region III and A_n^I in region II, as:

$$A_m^{III} = \sum_{n=-\infty}^{\infty} U_{n,m}^{*}\{\gamma_n r\} A_n^I , \tag{5.27}$$

here,
$$U_{nm}^{*}\{\gamma_n r\} = \left(\frac{2}{L-T}\right) \sum_{n=-\infty}^{\infty} \frac{B_2\{\gamma_n r\} S}{X_0'\{\gamma_m^{III} r\} \exp(j\omega t)} \quad . \tag{5.28}$$

Radial electric field is responsible for spoke formation in MILO during beam-wave interaction process. These spokes have RF energy that is stored inside the cavities. Thus, applying boundary conditions, given in Equation (5.8), to express field constant, A_n^I, in terms of circuit current.

$$E_r^{III} - E_r^{II} = \frac{\rho_s}{\varepsilon} = \frac{1}{\varepsilon}\left(\frac{q}{A}\right) = \frac{I_\theta}{2\pi r_d \varepsilon},$$

where the surface charge density ρ_s can be written as the ratio of total surface charge q to area A. Further, rearranging, and multiplying both sides by $\sin(\beta_m^{III} z)$ and integrated between the limit $0 \le z < (L-T)$,

$$\int_0^{(L-T)} (E_r^{III} - E_r^{II}) \sin(\beta_m^{III} z)\, dz = \int_0^{(L-T)} \frac{I_\theta}{(2\pi r_d)\varepsilon} \sin(\beta_m^{III} z)\, dz \cdot \tag{5.29}$$

Substituting field expressions from Equations (5.14) and (5.16) in (5.29) and value of field constant from (5.27) in the above Equation. After rearranging, above expression is written in term of circuit current,

$$A_n^I = \sum_{n=-\infty}^{\infty} Q_{nm}^* \left\{\gamma_n^I r\right\} I_\theta \tag{5.30}$$

where $$Q_{nm}^* \left\{\gamma_n^I r\right\} = \frac{\cos(\beta_m^{II}(L-T))\gamma_n(L-T)}{4\pi r_d \varepsilon(L-T)[(-jB_2\{\gamma_n r\}S)]}. \tag{5.31}$$

In order to couple the field intensity present between electron sheath and interaction cavities, boundary condition explained through (5.9) is considered here. Thus, substituting Equation (5.30) in (5.9), results in expression for axial electric field intensity in term of circuit current expressed as:

$$E_z^I = W_{nm}^* I_\theta , \tag{5.32}$$

here, $$W_{nm}^* \left\{\gamma_n^I r\right\} = Q_{nm}^* \left\{\gamma_n^I r\right\} J_0\{G_{2n} r\}.$$

Equating Equations (5.24) and (5.32), to find the ratio of circuit potential and circuit current, V/I_θ. Substituted resulting expression in (5.26), to find the equivalent series inductance per unit length in terms of structure parameters as:

$$L_e\left\{\gamma_n^I r\right\} = \frac{1}{j\omega}\left(\frac{\beta_n}{\gamma_n^I}\right)^2 Q_{nm}^* \left\{\gamma_n^I r\right\} J_0\{G_{2n} r\}. \tag{5.33}$$

5.3.3 Phase velocity of the structure

This is an important propagation parameter for the analysis and design of the slow-wave RF interaction structure. The phase velocity v_p of coaxial disc loaded structure can be calculated using the well known relation:

$$v_p = 1/(L_e C_e)^{1/2}. \tag{5.34}$$

Substituting the expressions of the equivalent shunt capacitance from Equation (5.25) and series inductance per unit length from Equation (5.33), the phase velocity can be obtained. Equations, obtained represents a set of homogeneous linear equations, the vanishing determinant of which, as a condition of the non-trivial solution, gives the dispersion relation of the structure.

5.3.4 Dispersion relation and Temporal growth rate

Dispersion relation is used for investigating the electromagnetic behavior or oscillation region for the RF interaction region of the MILO structure in the presence of the electron beam and is written as:

$$\beta = \omega\sqrt{L_e C_e}$$

Above equation represents dispersion relation. On substituting value of series inductance per unit length (L_e) and shunt capacitance per unit length (C_e) and rearranging, dispersion relation is written as:

$$\sum_{n=-\infty}^{\infty} (\xi_{n,m}^{1} - \xi_{n,m}^{2}) = 0 \tag{5.35}$$

The above dispersion relation (5.35) is same as derived using a more involved and cumbersome field analysis approach, where

$$\xi_{n,m}^{I} = \frac{\cos(\beta_m^{III} d)}{2\pi \mathrm{r}_d(d)} \times \left[\frac{X_0\{\gamma_m^{III} r\}}{\phi_n (1 - bJ_0\{\gamma_n r_b\} Y_0\{\gamma_n r_b\}) J_0\{\gamma_n r\} + bJ_0^2\{\gamma_n r_b\} Y_0\{\gamma_n r\}} \right].$$

and $$\xi_{nm}^{2} = \frac{\cos(\beta_m^{III}(d))}{2\pi \mathrm{r}_d(j\omega\varepsilon)(d)} \times \frac{\gamma_n}{\phi_n} \left[\frac{X_0'\{\gamma_m^{III} r\}}{(1 - bJ_0\{\gamma_n r_b\} Y_0\{\gamma_n r_b\}) J_1\{\gamma_n r\} + bJ_0^2\{\gamma_n r_b\} Y_1\{\gamma_n r\}} \right].$$

The dispersion relation for RF interaction structure is obtained here, on applying the equivalent circuit approach and is used to plot the dispersion characteristics as well as study the role of structure parameters to control its shape. In above equations d is defined as d = (L-T). For finding the temporal growth rate, Equation (5.35) is differentiated with respect to ω, by substituting $\omega \to \omega_0 + \delta\omega$, on rearranging results:

$$\delta\omega = -\omega + \left[\left(\frac{\gamma_n}{j\varepsilon} \phi_n \frac{X_0'\{\gamma_m^{III} r\}}{X_0\{\gamma_m^{III} r\}} \times \left(\frac{1 - bJ_0\{\gamma_n r_b\} Y_0\{\gamma_n r_b\}) J_0\{\gamma_n r\} + bJ_0^2\{\gamma_n r_b\} Y_0\{\gamma_n r\}}{1 - bJ_0\{\gamma_n r_b\} Y_0\{\gamma_n r_b\}) J_1\{\gamma_n r\} + bJ_0^2\{\gamma_n r_b\} Y_1\{\gamma_n r\}} \right) \right]^{1/2} \tag{5.36}$$

Above equation represent expression for temporal growth rate (that is imaginary part of ω, shows that waves are unstable and they grow in amplitude, drawing energy from sheared velocity field of relativistic Brillouin flow.

5.4 Expression for RF energy and temporal power growth

In this section RF energy stored and transfer through the slow wave structure is calculated using equivalent circuit approach. Admittance of the cavity [Dwivedi and Jain (2014)] can be written as:

$$Y(\omega) = \frac{1}{R}\left[1 + jRC\omega_0\left(\frac{\omega}{\omega_0} - \frac{\omega_0}{\omega}\right)\right].$$

$$\Rightarrow \qquad Y(\omega) = \frac{1}{R}\left[1 + jQ_{\text{int}}\left(\frac{\omega}{\omega_0} - \frac{\omega_0}{\omega}\right)\right]. \tag{5.37}$$

Here, $Q_{\text{int}} = RC\omega_0$ represents over-voltage coefficient or internal quality factor of cavity, due to dissipative losses in the walls [Cousin *et al.* (2005)]. Imaginary part of admittance represents energy stored or released from the cavity. Due to resonant frequency ω_0, the external over-voltage coefficient or external quality factor is written as, $Q_{ext} = \frac{Z_0}{\omega_0 L} = Z_0 C\omega_0$, here, Z_0 represents output impedance of the signal source. In MILO, energy stored inside cavity is coupled with the load through coaxial line with the output opening axially [Cousin *et al.* (2005)]. Interaction cavities coupling with the load may be either over coupling or under coupling depends upon the external and internal Q-factor. Coupling coefficient of the cavity is defined as,

$$\frac{Q_{ext}}{Q_{\text{int}}} = \frac{Z_0}{R} = \alpha. \tag{5.38}$$

For impedance matching if a transmission line is connected between source and load together, it must also be same impedance, $Z_0 = Z_i = Z_c$, where Z_c is the coupling impedance of the transmission line. During resonance when, $\alpha = 1$, $Z_c = Z_0$, the output guide is adapted with cavity and system behaves like an equivalent resonator or all electromagnetic energy injected is dissipated in cavity equivalent resistance.

Power transferred with the load is written as,

$$P = P_0(1 - \rho\bar{\rho}) \quad , \tag{5.39}$$

where, P_0 is initial power injected and ρ represents complex reflection coefficient function of the load impedance Z_c and of guide characteristic impedance Z_0 such as,

$$\rho = \frac{Z_0 - Z_c}{Z_0 + Z_c} = \frac{Y_c - Y_0}{Y_c + Y_0} \quad . \tag{5.40}$$

Substituting Equations (5.37) and (5.38) in (5.40),

$$\rho = \frac{(\alpha^2 - 1) + \alpha^2 Q_{\text{int}}^2 (\frac{\omega}{\omega_0} - \frac{\omega_0}{\omega})^2 + 2j\alpha Q_{\text{int}} (\frac{\omega}{\omega_0} - \frac{\omega_0}{\omega})}{(\alpha + 1)^2 + \alpha^2 Q_{\text{int}}^2 (\frac{\omega}{\omega_0} - \frac{\omega_0}{\omega})^2} \quad . \tag{5.41}$$

Multiply Equation (5.41) by its complex and after simple algebra,

$$(1 - \rho\bar{\rho}) = \frac{P}{P_0} = \frac{4\alpha}{(\alpha + 1)^2 + \alpha^2 Q_{\text{int}}^2 (\frac{\omega}{\omega_0} - \frac{\omega_0}{\omega})^2} . \tag{5.42}$$

Omitting α in expression,

$$\frac{P}{P_0} = \frac{4(Q_{ext} / Q_{\text{int}})}{(1 + Q_{ext} / Q_{\text{int}})^2 + Q_{ext}^2 (\frac{\omega}{\omega_0} - \frac{\omega_0}{\omega})^2} \quad . \tag{5.43}$$

Empty over-voltage coefficient, $Q_0 = \omega_0 \frac{W}{dW / dt}$

$$\frac{P}{P_0} = \frac{4Q_{ext} (\frac{1}{Q_{\text{int}}} + \frac{1}{\omega_0 W} \frac{dW}{dt})}{[1 + Q_{ext} (1 / Q_{\text{int}} + 1 / \omega_0 W (dW / dt)]^2 + Q_{ext}^2 (\omega / \omega_0 - \omega_0 / \omega)^2} \tag{5.44}$$

Power seen by cavity is the sum of the variation of energy stored during *dt* and of the power dissipated ($\omega_0 W / Q_{\text{int}}$) in the walls of disc,

$$P = \frac{dW}{dt} + \frac{\omega_0 W}{Q_{\text{int}}}, \tag{5.45}$$

$$\Rightarrow \quad \frac{P}{\omega_0 W} = \frac{1}{Q_{\text{int}}} + \frac{1}{\omega_0 W}\frac{dW}{dt} \quad . \tag{5.46}$$

Equation (5.46) can be rewritten after apply condition of resonance,

$$P = \sqrt{\frac{4P_0\omega_0 W}{Q_{ext}}} - \frac{\omega_0 W}{Q_{ext}}. \tag{5.47}$$

Equating equations (5.45) and (5.47), results in first order differential equation:

$$\frac{dW}{dt} + \frac{\omega_0}{Q_0}W - \sqrt{\frac{4P_0\omega_0}{Q_{ext}}}\sqrt{W} = 0. \tag{5.48}$$

Dividing above equation by ($W^{1/2}$), above equation becomes,

$$\frac{d(W^{1/2})}{dt} + \frac{\omega_0}{2Q_0}W^{1/2} - \sqrt{\frac{P_0\omega_0}{Q_{ext}}} = 0 \ . \tag{5.49}$$

General solution of above equation,

$$W(\mathrm{t}) = \frac{4P_0Q_0^2}{\omega_0 Q_{ext}}\left[1 - \exp\left(-\left(\frac{\omega_0}{2Q_0}t\right)\right)\right]^2, \tag{5.50}$$

$$\Rightarrow \quad W(t) = W_0\left[1 - \exp\left(-\frac{\omega_0}{2Q_0}t\right)\right]^2, \tag{5.51}$$

where, $\omega_0 = 1/\sqrt{L_e C_e}$ and $W_0 = 4P_0Q_0^2 / \omega_0 Q_{ext}$. Q_0 is the loaded quality factor and is proportional to energetic storage characteristic time inside the slow wave structure [Cousin *et al.* (2005)]. W_0 is the maximum energy stored inside the resonator. RF energy developed through the MILO device is calculated using expression (5.51) on substituting expression for inductance and capacitance per unit length. Temporal RF output power developed during beam-wave interaction process is calculated by

substituting (5.51) in (5.47), thus released RF energy is used to calculate RF output power from the device.

5.5 Results and Discussion

To achieve efficient conversion of energy to RF, from electron sheath that is magnetically insulated (consist of stream of free electrons) to electromagnetic radiation, near synchronism must be attained between velocity of electrons and phase velocity of waves. This condition is established in crossed field device MILO, by reducing velocity of electromagnetic waves wave, by a slow wave structure comprising of periodic arrangement of resonant cavities. Cylindrical configuration of MILO allows for a continuous circulation of growing electromagnetic wave and thus system provides its own internal feedback. In the presence of electron beam inside the RF structure, generated instability due to beam-wave interaction produces complex frequency and wavenumber that is responsible for temporal growth rate. In order to predict the oscillation in MILO using equivalent circuit approach, dispersion relation having real and imaginary part is solved numerically for defined structure and beam parameters. For validation of our result of temporal growth rate, we find our result in agreement with reported result using field analysis case [Dwivedi and Jain (2012)].

5.5.1 Effect of structural parameters on propagation characteristic

Disc loaded coaxial structure exhibiting certain propagation characteristics of transmission line parameters due to distributed capacitance and inductance along its length. It can be seen from Figure 5.2 (a), for the defined structure and beam parameters, referred from [Dwivedi and Jain (2013)], the distributed capacitance will increase until a certain resonant frequency and the distributed inductance will decreases, acquire a dip at maximum resonant frequency. Increases the shunt

capacitance and decreases the series inductance, both changes result in a larger current drawn that helps in proper spoke formation during beam-wave interaction mechanism. Thus, current develop for a given applied voltage, equating to a lesser impedance. As can be seen from Figure 5.2, an increasing pattern of shunt capacitance, helps to understand the concentration of the electric field on the beam axis that further increases the transit time factor. Increasing pattern of capacitance, means inductance has to be lowered to maintain the same resonant frequency and this can be observed from Figure 5.2. Series inductance goes down because the amount of magnetic energy stored is reduced, results in increase of current, that further helps in magnetic insulation process. For the typically chosen structure parameters and chosen coaxial waveguide mode, in Figure 5.2(b) variation of the series inductance with frequency is plotted. It can be further observed from Figure 5.2, there exists typical electromagnetic coupling from one cavity to another and this is due to the capacitive coupling at the bottom of resonance cavities and weak mutual inductance coupling at the top.

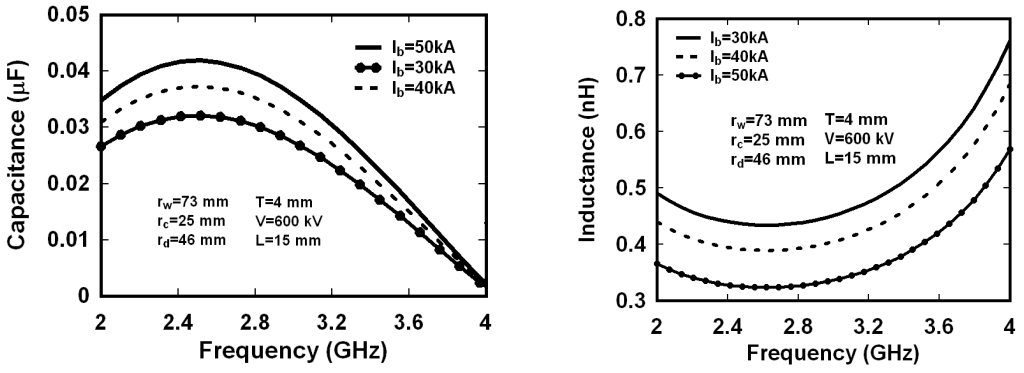

(a) **(b)**

Figure 5.2: Variation of **(a)** shunt capacitance and **(b)** series inductance per unit length versus frequency plot.

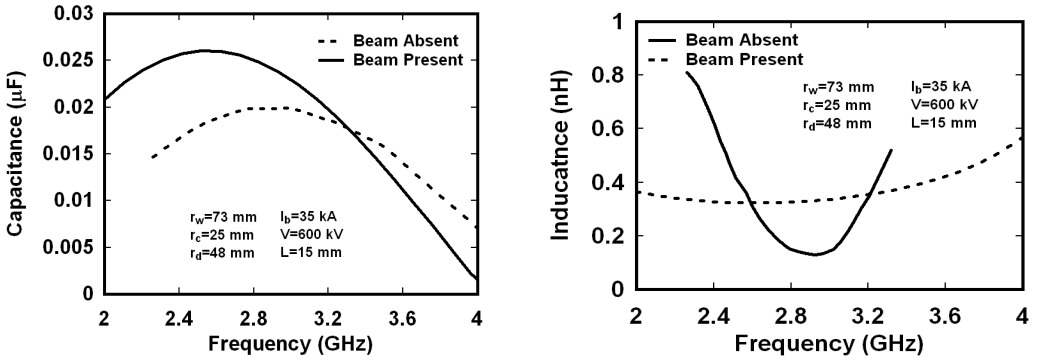

(a) **(b)**

Figure 5.3: Comparison plot representing variation of **(a)** shunt capacitance and **(b)** series inductance per unit length versus frequency for beam absent and beam present case.

Considering beam absent analysis defined in previous chapter, Figure 5.3 represent comparison plot. It is concluded from Figures 5.3(a) and (b), that due to presence of beam, there is slight difference in shunt capacitance and series inductance per unit length. This effect arises due to presence of space charge waves between tip of disc and the cathode.

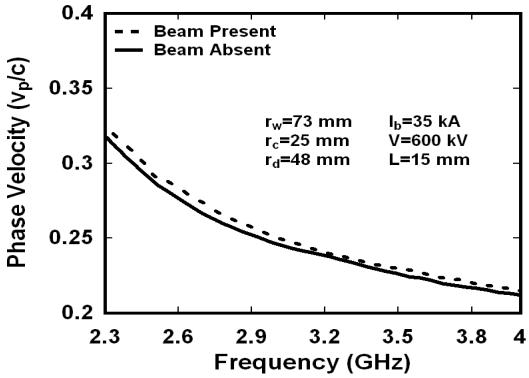

Figure 5.4: Variation of phase velocity versus frequency plot of disc loaded coaxial waveguide.

To attain efficient beam-wave interaction inside the structure, phase velocity should remain constant with frequency, as seen from Figure 5.4. Considering beam absent analysis defined in previous chapter, Figure 5.3 represent comparison plot. It is concluded from Figures 5.3(a) and (b), that due to presence of beam, there is slight

difference in shunt capacitance and series inductance per unit length. This effect arises due to presence of space charge waves between tip of disc and the cathode. Absolute part of capacitance and inductance is considered during analysis. Effect of real and imaginary part of the shunt capacitance and series inductance per unit length will be considered for future studies.

Figure 5.2 represents variation of shunt capacitance and series inductance with respect to frequency for different beam current. With increase in beam current, instability in the device grows faster, electrons present at the sheath boundary will undulate under the perturbing field, represents space charge waves. These space charge waves led to instability, known as Diocotron instability that occurs in neutralised charge sheets in the presence of uniform magnetic field. It can be inferred from figure 5.2(a), that shunt capacitance decrease with increase of beam current, keeping all other structure and beam parameters constant, further helps in compensating oscillations inside the interaction cavity. These oscillations are due to space charge waves oscillating at plasma frequency. Due to shunt capacitance, synchronism condition occurs and cavity resonates at a particular operating frequency. Behaviour of series inductance from Figure 5.2(b), speculates that energy exchange between beam and RF occurs due to increasing behaviour of curve, resulting in spoke formation. Efficient beam-wave interaction process is revealed properly from the temporal growth rate, which is defined by the imaginary component of frequency corresponding to conjugate roots of the dispersion relation. Using dispersion relation interaction of electron beam with the phase velocity of electromagnetic mode through the slow wave structure has been explained properly. For zero beam current, the dispersion passes onto to the beam absent dispersion relation of the disc-loaded coaxial structure, as reported earlier by the authors.

Considering this analysis, starting threshold for the occurrence of instability is explained properly, if structure and beam parameters are satisfying the above relation. In order to determine temporal growth rate and dispersion relation, a typical structure and beam parameter selected for MILO, [Dwivedi and Jain (2012)]. Considering Equation (5.36), on plotting graph between temporal growth rate versus wave number, one can realizes oscillation region in MILO due to which instability takes place. Due to this instability beam-wave interaction mechanisms occur. Instability can occur where slow TM_{0n} waves intersect space charge modes, because at this point they have equal phase velocities.

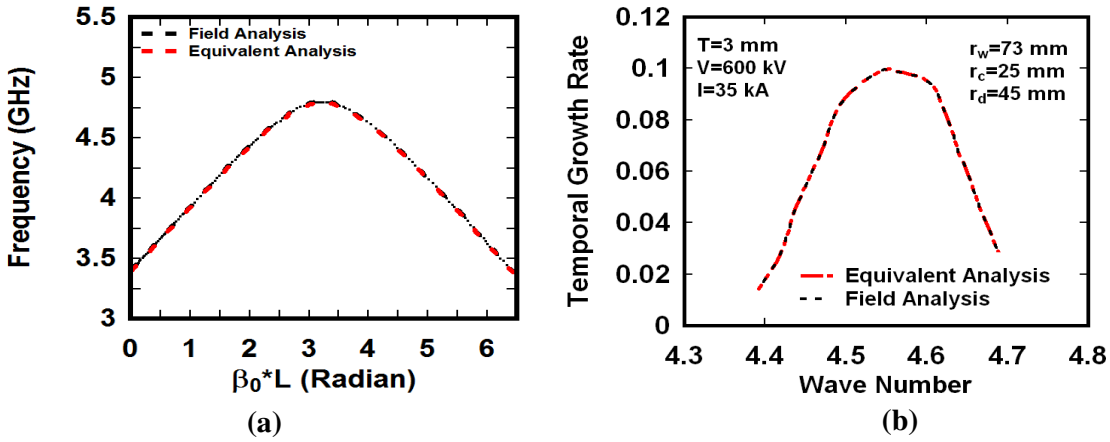

Figure 5.5: **(a)** Dispersion versus frequency plot for TM_{01} mode at beam voltage 600 kV and beam current 35 kA, **(b)** Variation of Temporal growth rate with wave number.

To validate the result obtained through equivalent circuit approach, authors have taken resort of published result of [Dwivedi and Jain (2012)] where the device parameters taken are shown in Figure 5.5(b). The real part of the root of dispersion relation has been obtained numerically and corresponding plot obtained is shown in Figure 5.5(a). Results obtained are closely agree with those obtained using the field analytical approach. It is inferred from Figure 5.5 (b), that the device instability region lies between 4.54 cm^{-1} and 4.76 cm^{-1}.

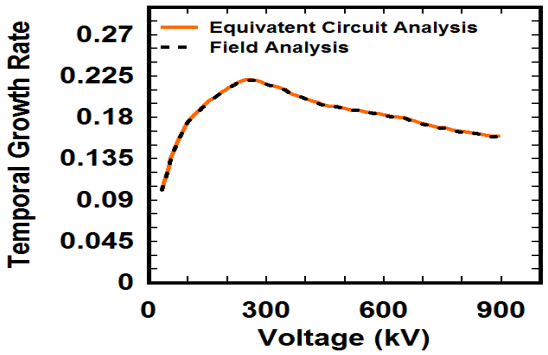

Figure 5.6: Plot of the temporal growth rate versus voltage.

It can be seen from Figure 5.6 that for the typical device parameter selected, temporal growth rate does not change significantly for applied voltages, due to compensation provided by the shunt capacitance and series inductance.

5.5.2 Variation of RF energy and Output power

Electromagnetic RF energy stored inside the RF interaction cavity supporting a transverse magnetic mode can be calculated by equivalent circuit analysis considering admittance of the circuit [Dwivedi and Jain *(*2014)]. Resonant frequency is calculated by considering series inductance and shunt capacitance per unit length. Therefore, the RF energy is being calculated in terms of input power in the cavity and its quality factor. For proper functioning, resonator cavity or slow wave structure of MILO must store electromagnetic energy, that is sufficient to exchange RF energy with the beam. At a particular resonant frequency, the conditions are necessary to store maximum energy as shown in Figure 5.7 below. Figure 5.7(a) reveals information related to maximum energy stored, and the time needed to stored energy, which contributes during beam-wave interaction process. This released RF energy is further used to calculate RF output power during beam-wave interaction process considering Equations (5.47) and (5.51).

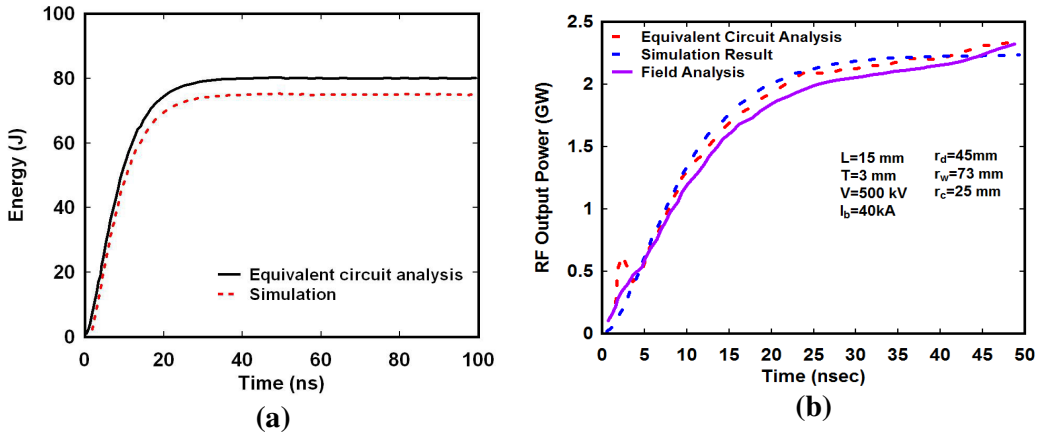

Figure 5.7: (a) Variation of RF energy versus time, **(b)** Variation of RF output power versus time.

In order to validate the analytical approach developed with the field analysis, the RF energy and RF output power released during beam-wave interaction behavior have been shown in Figure 5.7(a) and 5.7(b) for the selected structure and beam parameters [Dwivedi and Jain (2012)]. The analytical results obtained are in agreement with the simulation result ± 5%.

5.6 Conclusion

The equivalent circuit approach has been developed considering the presence of electron beam in order to study RF analysis of MILO. This approach has been used to investigate the device oscillation condition, dispersion relation and temporal RF growth rate. The developed simplified dispersion relation result and temporal RF growth rate result has been validated against the published results as well as values obtained through simulation. RF energy stored during beam-wave interaction is numerically analyzed using admittance of the cavity and considering the effect of quality factor. Effect of various structure parameters, such as coaxial disc hole radius, periodicity between discs and beam radius on the shunt capacitance and series inductance per unit length, have also been discussed.